This article has been accepted for publication in a future issue of this journal, but has not been fully edited. Content may change prior to final publication. Citation information: DOI 10.1109/TPWRS.2020.3036448, IEEE Transactions on Power Systems

Inclusion of Battery SoH Estimation in Smart Distribution Planning with Energy Storage Systems

Omar Alrumayh†, *Student Member, IEEE*, Steven Wong‡, *Member, IEEE*, and Kankar Bhattacharya†, *Fellow, IEEE*

***Abstract*—Energy storage systems (ESSs) can improve energy management in distribution grids, especially with the increasing penetration of home energy management systems (HEMSs) that schedule household appliances and render them as smart loads. A large number of uncoordinated HEMSs can result in significant changes to the aggregated load profile of the distribution system. This paper proposes a framework and mathematical model for integrating ESS in the distribution grid to minimize the operation cost of the local distribution company (LDC) and alleviate the impact of uncoordinated HEMS operation on the distribution grid. A novel neural network (NN) based state of health (SoH) estimator for a lithium-ion (Li-ion) battery based ESS is proposed, which is incorporated within the LDC's planning problem. The results show that the proposed estimation model is an accurate estimation of the SoH of the ESS. The LDC's planning decisions are also compared, considering SoH of the ESS vis-á-vis linear degradation and no-degradation models.**

***Index Terms*—Degradation, energy storage system, home energy management system, local distribution company, smart grid, state of health, distribution planning.**

NOMENCLATURE

LDC Operations and Planning Model with ESS

Indices and Sets

h_j	Index of houses, $h_j \in \mathcal{H}$
j, k	Index of buses in distribution system, $(j, k) \in \mathcal{N}$
n, y	Index of year, $(n, y) \in Y$
t	Index of time, $t \in \mathcal{T}$

Parameters

C_P^{F}	Fixed installation cost of ESS, \$
$C_P^{\mathrm{V}}, C_E^{\mathrm{V}}$	Variable installation cost of ESS associated with power (\$/kW) and energy (\$/kWh), respectively
$C^{\mathrm{OM_F}}$	Fixed operation and maintenance cost of ESS, \$/kW-year
$C^{\mathrm{OM_V}}$	Variable operation and maintenance cost of ESS, \$/kWh
C^{REP}	Replacement cost of ESS, \$/kW
DOD_j	Depth of discharge limit of ESS j, $p.u$
DY	Number of seasonal representative days
$\underline{EPR}, \overline{EPR}$	Limits of energy to power ratio
HY	Number of hours per year, h
$P^d_{j,y,t}$	Residential load demand, $p.u$
$P^{\min}, P^{\max}$	Power limits of distribution substation, $p.u$
$P^{\mathrm{STD}}, E^{\mathrm{STD}}$	Standard power/energy capacity of ESS available in market
R	Discount rate, %
$V^{\min}, V^{\max}$	Voltage limits, $p.u$
α_{DOD}	Maximum allowable change in state of charge (SoC)
η^{CH}/η^{DCH}	Charging and discharging efficiency of ESS, %
$\Upsilon_{y,t}$	Electricity price, \$/kWh

Variables

$E_{j,y,t}$	Actual energy capacity of ESS, $p.u$
J_1, J_2, J_3	ESS installation, operation, and replacement cost, respectively, \$.
NU^P, NU^E	Integer multiplier of standard size of ESS
$OT_{j,y,t}, OY_{j,y}$	Number of hours/years ESS in service, respectively
$P^{SS}_{j,y,t}, Q^{SS}_{j,y,t}$	Active/reactive power drawn from substation, $p.u$
$P^d_{j,y,t}, Q^d_{j,y,t}$	Active/reactive power demand from residential loads, $p.u$
$P^{INST}_{j,y}, E^{INST}_{j,y}$	Installed power/energy capacity of ESS, $p.u$
$P^{Rate}_{j,y}, E^{Rate}_{j,y}$	Rated power/energy capacity of ESS, $p.u$
$P^{CH}_{j,y,t}, P^{DCH}_{j,y,t}$	Active power to be charged/discharged to/from ESS, $p.u$
$SoC_{j,y,t}$	State of charge of ESS, $p.u$
$\widehat{SoH}_{j,y,t}$	Estimated SoH of ESS, %
$V_{j,y,t}$	Voltage at bus, $p.u$
$Z^{INST}_{j,y}, Z^{REP}_{j,y}$	Binary installation and replacement decisions of ESS, respectively.
$Z^{PI}_{j,y}, Z^{PR}_{j,y}$	Binary presence indicator of ESS after installation / replacement.
$\overline{\Delta SoC}_{j,y,t}$	Maximum allowable change in $SoC_{j,y,t}$, $p.u$
$\delta_{j,y,t}$	Voltage angle at bus, $p.u$

Degradation Model

Indices and Sets

$\mathtt{K}$	Index of cycle, $\mathtt{K} \in \mathcal{K}$

Parameters

$\delta_{\mathtt{K}}$	Depth of discharge of $\mathtt{K}^{th}$ cycle
$\sigma_{\mathtt{K}}$	State of charge of $\mathtt{K}^{th}$ cycle
$T_{\mathtt{K}}$	Ambient temperature during $\mathtt{K}^{th}$ cycle
$\beta_{sei}, \alpha_{sei}$	Parameters of the early degradation model

Variables

f_t, f_c	Calendar and cycle aging, respectively
f_{sei}	Degradation function of ESS during early cycles

†Department of Electrical and Computer Engineering, University of Waterloo, Ontario, Canada (e-mail: oalrumayh, kankar@uwaterloo.ca).
‡Natural Resources Canada, CanmetENERGY, Varennes, Quebec, Canada, (e-mail: steven.wong@canada.ca).
O. Alrumayh is also with the Department of Electrical Engineering, College of Engineering, Qassim University, Unaizah, Saudi Arabia.

The first author acknowledges the financial support from Qassim University, Saudi Arabia, and Saudi Arabian Culture Bureau, Ottawa, Canada, to carry out this research. The work was also financially supported by NSERC (Canada) Energy Storage Technology (NEST) Network (website: www.ryerson.ca/nestnet/).

0885-8950 (c) 2020 IEEE. Personal use is permitted, but republication/redistribution requires IEEE permission. See http://www.ieee.org/publications_standards/publications/rights/index.html for more information.
Authorized licensed use limited to: University of Waterloo. Downloaded on April 14,2021 at 09:42:43 UTC from IEEE Xplore. Restrictions apply.

f_d	Degradation function of ESS
$SoH_{j,y,t}$	Actual SoH of ESS, %
a_{K}	Cycle indicator, $[0.5, 1]$

Neural Network Model

Indices and Sets

i	Index of input, $i \in I$
o	Index of hidden layer neuron, $o \in O$

Parameters

β_o, Γ	Hidden/output layer neuron bias
$n^{in}_{o,j,y,t}, n^{out}_{o,j,y,t}$	Input and output of a hidden layer neuron
$w_{i,o}, W_o$	Input weight and layer weight, respectively
$x^{i}_{j,y,t}, x^{i,N}_{j,y,t}$	Actual and normalized input i
$X_{j,y,t}, X^{N}_{j,y,t}$	Actual and normalized output of NN

I. Introduction

POWER systems are experiencing changes in energy generation and consumption with the movement towards a smart grid and increased penetration of distributed renewables. An important component of the smart grid are home energy management systems (HEMSs), which help residential customers optimize their consumption. However, HEMSs can significantly influence the system load profile, and thus there is a need for their coordinated operation, as discussed in the authors' earlier work [1]. In practice though, there are significant numbers of HEMSs which operate in an uncoordinated manner.

One of the issues which may arise with uncoordinated HEMSs is the appearance of large demand spikes during low time-of-use (TOU) price periods [2]. Therefore, researchers have proposed different control strategies for residential loads [3]–[5] to mitigate the impact of the effect on distribution operation. In [3], a direct load control approach is proposed to optimally manage the number of residential heating, ventilation, and air conditioning (HVAC) systems and community energy storage systems (ESSs) to mitigate the impact of high demand during demand response (DR) events. In [4], a hierarchical control strategy is proposed to coordinate the operation of multiple HVAC units in order to flatten the system load profile. Another work [5] proposes a coordination scheme between HEMSs and the grid EMS to optimally charge / discharge electric vehicles (EV) to minimize HEMS total operation cost and photovoltaic (PV) curtailment. In [6], a day-ahead decentralized scheduling algorithm is proposed to coordinate HEMSs and hence maximize the use of distributed energy resources (DERs). While these earlier papers proposed strategies to coordinate HEMSs, this paper considers the presence of uncoordinated HEMSs and investigates mitigating their impact on the local distribution company (LDC)'s distribution system planning with ESSs.

There is a growing body of literature on integrating ESS into the distribution grid to assist the LDC in managing grid operations. The technical and economic advantages include increasing the operating margins to facilitate renewable energy sources (RESs) and EVs penetration [7] and deferring upgrades to the distribution grid. The authors in [8] propose a multi-objective optimization approach to optimally site distributed generation (DG) units, ESSs, and RESs. An optimal planning approach is proposed in [9] and [10] to determine the location, rated energy and power capacity of battery ESS to mitigate the impact of uncertainty associated with renewable-based DG. In [11], a genetic algorithm-based planning framework is proposed to size and site ESSs in a distribution grid in order to minimize system losses, defer system upgrades, and maximize profit from energy arbitrage. Another work [12] proposes a stochastic approach to coordinate the planning of ESSs and RESs while considering DR. In [13], a chance-constrained approach is proposed for ESSs planning in a distribution grid. However, none of the above works have considered the lifetime of the ESSs nor the impact of degradation on the asset's operation.

Several researchers have considered degradation of the ESSs [14]–[19], but for different studies. In [14], an operational planning scheme is proposed to coordinate wind farms with ESSs to mitigate impact of wind forecast errors and extend lifetime of the ESS batteries by reducing frequent charges/discharges. A multi-stage approach is proposed in [15] to optimally plan for transmission expansion and ESS deployments considering a linear degradation rate of the batteries. In [16], a decomposition approach is proposed to optimally determine the size and year of installation of ESS in a microgrid while assuming an annual degradation factor of the batteries. A battery ESS sizing model is proposed in [17] to optimally determine the size and the number of units required to minimize the microgrid operation cost and unserved energy cost. In [18], the authors propose a planning model for isolated microgrids considering re-purposed EV batteries, assuming a linear change in the ESS's state of health (SoH) due to calendar and cycle aging. In [19], the participation of ESS in frequency regulation in the PJM market is assessed considering the impact of different depth of discharge levels on the SoH of various types of lithium-ion (Li-ion) batteries.

In this work, a novel neural network (NN)-based degradation model is developed to estimate the SoH of Li-ion batteries, which is then embedded within a distribution system planning model to determine the optimal sizing, siting, year of installation / replacement of Li-ion based ESSs. The main objective of the LDC is to minimize the net present value of its ESS investment, replacement and system operation cost, while respecting technical constraints such as active and reactive power balance, bus voltage limits, and substation capacity.

The degradation model of [19], used here, is based on Rainflow Algorithm (RFA). However, since distribution system planning problems with ESS must simultaneously compute state of charge (SoC) profiles based on ESS operational decisions and the optimal ESS plan, RFA-based degradation models [19] cannot be implemented directly within these models. To address this problem, a novel SoH estimation approach for an ESS in a distribution system is proposed in this paper that does not require the RFA.

The proposed NN-based approximation of the degradation

0885-8950 (c) 2020 IEEE. Personal use is permitted, but republication/redistribution requires IEEE permission. See http://www.ieee.org/publications_standards/publications/rights/index.html for more information.
Authorized licensed use limited to: University of Waterloo. Downloaded on April 14,2021 at 09:42:43 UTC from IEEE Xplore. Restrictions apply.

This article has been accepted for publication in a future issue of this journal, but has not been fully edited. Content may change prior to final publication. Citation information: DOI 10.1109/TPWRS.2020.3036448, IEEE Transactions on Power Systems

model is an important contribution as it captures the SoH of Li-ion batteries more precisely than other methods in the literature. This SoH function is then embedded within the distribution planning problem, which thereby overcomes the issue of under- or over-estimating ESS capacity resulting in over- or under-capacity planning in the distribution system, as was an issue in earlier works [15], [16], [18]. Furthermore, the SoH function approximation approach presented in this paper is not limited to distribution planning problems: researchers can use this concept and SoH model for distribution system operations, ESS incentive design, ESS market participation, and other applications.

In view of the above discussions, the main contributions of this work are as follows:

- A novel NN based degradation model is proposed to estimate the SoH of Li-ion batteries of an ESS by considering a large data set of ESS operations for NN training. This data set is obtained by simulating the LDC behavior in controlling ESS in the presence of a large cluster of uncoordinated HEMS loads.
- The proposed SoH model of the ESS is incorporated into the distribution planning model to determine the optimal energy capacity, power rating, location and year of installation / replacement of ESSs while internalizing ESS battery capacity degradation due to cycling and aging effects.

The rest of the paper is organized as follows: Section II discusses the components of the proposed planning framework and the associated mathematical models. The simulation results and discussions are presented in Section III. The main conclusions of the work are presented in Section IV.

II. Proposed Planning Framework and Mathematical Models

The proposed ESS planning framework considering the inclusion of a Li-ion battery SoH estimation model is presented in Fig. 1. The framework comprises the following steps:

- The residential energy hub (REH) operations model (discussed in Section II.A) and based on [1] is executed to develop bus-wise load profiles. These load profiles are used to simulate an LDC operations model (discussed in Section II.B) to obtain a set of SoC profiles of the ESS.
- Using the RFA (discussed in Section II.C) on these SoC profiles, the Li-ion based ESS cycle parameters are determined, which are input to a degradation model [19] to obtain the actual SoH (discussed in Section II.D).
- The SoC and SoH profiles, so obtained, are used to train a NN, and the function relationship of the SoH is extracted (discussed in Section II.E).
- This functional relationship is included in the LDC planning model to determine the optimal plan decisions. The estimated SoH profiles obtained from the planning model are send back to the NN-based estimator to re-train and improve the SoH estimation function for revising the plan decisions. The framework arrives at the optimal plan when the mismatch in the estimation of SoH with the actual, is minimal.

A. REH Operations Model

The HEMS are residential controllers that carry out scheduling of the REH including all house appliances and power interchanges with the external grid, considering the customer's preferences and objectives, such as minimizing its daily energy cost. In this work, the REH operations model is taken from [1], and simulated for daily load profiles over a 10 year horizon (i.e. 365 x 10 days).

B. LDC Operations Model

After completing the simulation of all REHs, bus-wise load profiles are created over a period of ten years. The LDC operations model including ESS is then simulated to analyze the operational decisions of the ESS.

1) Objective Function: minimize LDC's daily operation cost, comprising the cost of importing power from external grid at electricity price $\Upsilon_{y,t}$ to meet the residential load demand.

$$J = \sum_{y=1}^{Y} \Upsilon_{y,t} P^{SS}_{j=1,y,t} \tag{1}$$

subject to the following constraints:

2) Load Flow Equations: Linearized power flow equations, as in [20] are used:

$$\begin{aligned} &P^{SS}_{j,y,t} - P^{d}_{j,y,t} + (P^{DCH}_{j,y,t} - P^{CH}_{j,y,t}) = \\ &\sum_{k=1,k\neq j}^{\mathcal{J}} \Big(K_{j,k,1}(\delta_{j,y,t} - \delta_{k,y,t}) + K_{j,k,2}(V_{j,y,t} - V_{k,y,t}) \Big) \end{aligned} \tag{2}$$

$$\begin{aligned} &Q^{SS}_{y,t} - Q^{d}_{j,y,t} = \\ &\sum_{k=1,k\neq j}^{N} K_{j,k,2}(\delta_{j,y,t} - \delta_{k,y,t}) + K_{j,k,1}(V_{j,y,t} - V_{k,y,t}) \end{aligned} \tag{3}$$

where,

$$K_{j,k,1} = \frac{\frac{x^2_{j,k}}{r^2_{j,k}+x^2_{j,k}}}{x_{j,k}}, K_{j,k,2} = \frac{\frac{r_{j,k}x_{j,k}}{r^2_{j,k}+x^2_{j,k}}}{x_{j,k}},\ \forall (j,k) \in \mathcal{J} \tag{4}$$

These are subject to bus voltage constraints and limits on power drawn from the substation, as given below:

$$V^{\min}_{j} \leq V_{j,y,t} \leq V^{\max}_{j} \tag{5}$$

$$P^{\min} \leq P^{SS}_{j=1,y,t} \leq P^{\max} \tag{6}$$

The following equations present the operational constraints of the ESS:

$$SoC_{j,y,t+1} = SoC_{j,y,t} + \eta^{CH} P^{CH}_{j,y,t} - \frac{P^{DCH}_{j,y,t}}{\eta^{DCH}} \tag{7}$$

$$-\overline{\Delta SoC}_{j,y,t} \leq SoC_{j,y,t} - SoC_{j,y,t-1} \leq \overline{\Delta SoC}_{j,y,t} \tag{8}$$

0885-8950 (c) 2020 IEEE. Personal use is permitted, but republication/redistribution requires IEEE permission. See http://www.ieee.org/publications_standards/publications/rights/index.html for more information.
Authorized licensed use limited to: University of Waterloo. Downloaded on April 14,2021 at 09:42:43 UTC from IEEE Xplore. Restrictions apply.

This article has been accepted for publication in a future issue of this journal, but has not been fully edited. Content may change prior to final publication. Citation information: DOI 10.1109/TPWRS.2020.3036448, IEEE Transactions on Power Systems

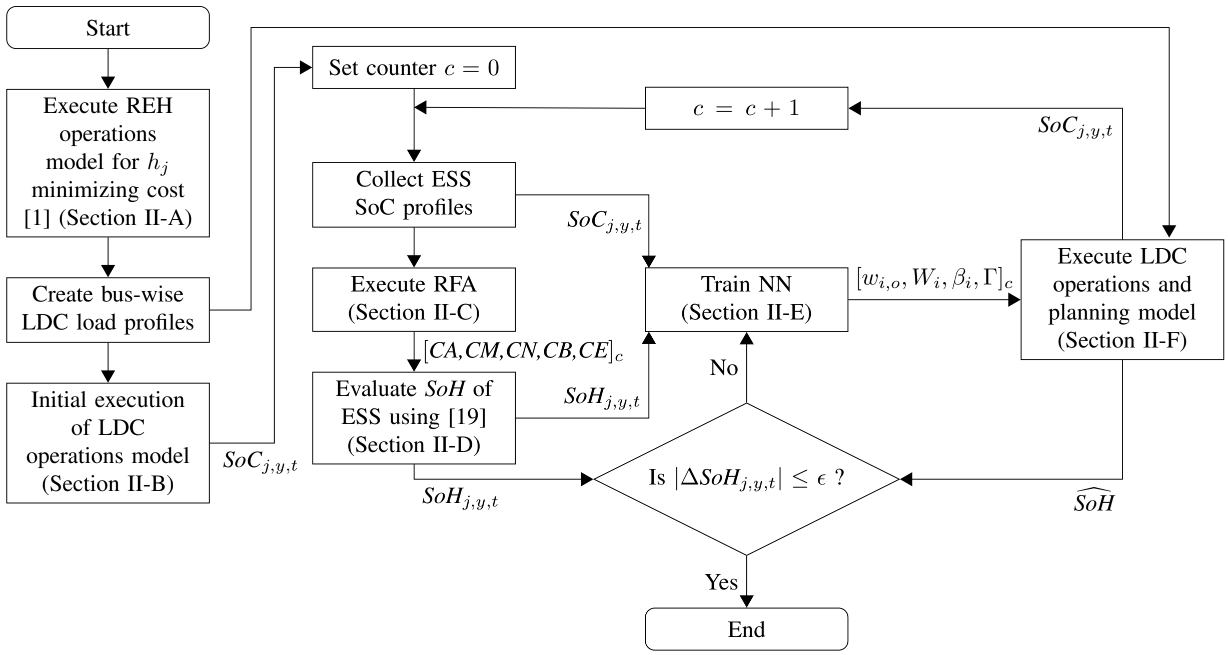

Fig. 1. Proposed ESS planning framework considering smart REHs and battery SoH.

where,

$$\overline{\Delta SoC}_{j,y,t} = \alpha_{DOD}\ E_{j,y,t} \tag{9}$$

The inter-temporal change in the SoC level is defined by (7), and the same is limited by minimum and maximum allowable changes, given by (8). Equation (9) states that the value of the maximum allowable change in SoC is a fraction, α_{DOD}, of $E_{j,y,t}$.

$$(1 - \overline{DoD})\ E_{j,y,t} \leq SoC_{j,y,t} \leq E_{j,y,t} \tag{10}$$

$$SoC_{j,y,t=1} = SoC_{j,y,t=24} = 0.5\ E_{j,y,t} \tag{11}$$

$$P^{CH}_{j,y,t} \leq P^{Rate}_{j,y} \tag{12}$$

$$P^{DCH}_{j,y,t} \leq P^{Rate}_{j,y} \tag{13}$$

In (10), the physical capacity of the ESS limits its SoC considering the maximum allowable Depth of Discharge (DoD). It is assumed that the SoC of the ESS at the beginning and end of the daily operation are equal, equation (11), to prevent the optimization model from choosing the maximum SoC at the beginning of the day and fully discharge at the end of the day. Moreover, the rated power of the ESS constraints the power charging/discharging capability from/to the ESS in (12) and (13).

C. RainFlow Algorithm

The RFA is a well known approach in the analysis of fatigue data [21]. It has been used in some recent works [22] and [23] for analysis of ESS operation, wherein the RFA counts the number of irregular cycles within a given operation period. The algorithm requires the SoC profile of the ESS as an input, as shown in Fig. 1, in order to obtain the following:

- Cycle amplitude (*CA*).
- Cycle mean value (*CM*).
- Cycle number (*CN*).
- Cycle begin and end times (*CB*, *CE*).

The results obtained from applying the RFA are used to calculate the variables of the degradation model, discussed next.

D. Degradation Model of ESS

In [19], a mathematical model was proposed to evaluate lithium-ion battery cell life considering calendar and cycle aging. Calendar aging represents the battery's inherent degradation over time, as a function of the average temperature ($\overline{T}$) and the average SoC of the battery ($\overline{\sigma}$). Cycle aging represents the loss of life due to the charging and discharging of the battery, represented as a function of the DoD, SoC, and temperature. This is given as follows [19]:

$$f_d(t, \delta, \sigma, T) = f_t(t, \overline{\sigma}, \overline{T}) + \sum_{\mathtt{K}}^{\mathcal{K}} a_k f_c(\delta_{\mathtt{K}}, \sigma_{\mathtt{K}}, T_{\mathtt{K}}) \tag{14}$$

The first term in (14) represents the effect of calendar aging (f_t) while the second term represents the degradation as a result of cycle aging (f_c). In addition, ESS degradation during its operation in the early cycles is given by [19],

$$f_{sei} = \beta_{sei} f_d \tag{15}$$

The $SoH_{j,y,t}$ of ESS can be represented as follows:

$$SoH_{j,y,t} = 1 - \alpha_{sei} \cdot e^{-f_{sei}} - (1 - \alpha_{sei}) \cdot e^{-f_d} \tag{16}$$

where α_{sei} denotes the portion of the ESS capacity lost during the early operation. The third term in (16) represents the degradation due to calendar and cycle aging. In order to apply the degradation model (14)-(16) to irregular cycle operation of ESS, the outcomes of the RFA are used as inputs to the degradation model, as follows [19]:

0885-8950 (c) 2020 IEEE. Personal use is permitted, but republication/redistribution requires IEEE permission. See http://www.ieee.org/publications_standards/publications/rights/index.html for more information.
Authorized licensed use limited to: University of Waterloo. Downloaded on April 14,2021 at 09:42:43 UTC from IEEE Xplore. Restrictions apply.

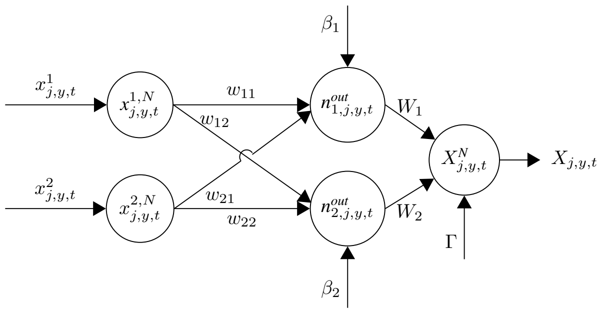

Fig. 2. Structure of the proposed NN-based SoH estimator.

- $\delta_{\mathtt{K}} = 2\ CA_{\mathtt{K}}$.
- $\sigma_{\mathtt{K}} = CM_{\mathtt{K}}$.
- $\overline{\sigma}$ = Average value of *CM*.
- $T_{\mathtt{K}}$ = Mean temperature between start and end time of $\mathtt{K}^{th}$ cycle.
- $\overline{T}$ = Mean value of the temperature profile.

The following subsection presents a novel SoH estimation approach (i.e. $\widehat{SoH}$) for an ESS in a distribution system that does not require RFA.

E. Proposed NN Based ESS SoH Estimator

This paper adopts the degradation model in [19] to propose a novel approach for estimating the SoH of the ESS. For this purpose, an NN-based mathematical model of the SoH is developed to be embedded within the distribution planning model in order to take into account the impact of calendar and cycle aging in determining the optimal ESS size, location, and operation decisions.

In order to estimate the SoH of ESS ($\widehat{SoH}$), a supervised learning technique is applied to train the NN with outcomes of the LDC operation of model, i.e., SoC profiles of 365 days for 10 years operation, as shown Fig. 1. The required output vector of the NN is the target SoH ($SoH_{j,y,t}$), which is determined as follows: (a) Use RFA to find *CA*, *CB*, *CE*, *CN*, and *CM*. (b) Calculate the input of the degradation model $\delta_{\mathtt{K}}$, $\sigma_{\mathtt{K}}$, $\overline{\sigma}$, $T_{\mathtt{K}}$, and $\overline{T}$, as discussed in Section II-D and shown in Fig. 1. (c) Evaluate the ESS SoH using the degradation model adopted in Section II-D, the output of which represents the target vector of the NN. As a result, a $[87,600\ \times\ 2]$ order matrix training set and a $[87,600\ \times\ 1]$ target vector are used for the NN training. Accordingly, the $\widehat{SoH}$ of an ESS located at bus (j) at year (y) and time (t) can be expressed as a function of SoC and operation time, as given below:

$$\widehat{SoH}_{j,y,t} = f(SoC_{j,y,t}, OT_{j,y,t}) \tag{17}$$

The NN has one hidden layer with two hidden layer neurons, which is obtained by trial-and-error; the NN is trained using Marquardt learning technique in MATLAB [24]. The resulting structure of the NN-based SoH Estimator is shown in Fig. 2. The mathematical representation of the NN function is developed as follows:

- Pre-processing input: The inputs of the NN $x^i_{j,y,t} = \{SoC_{j,y,t}, OT_{j,y,t}\}$ are normalized to lie in the interval $[-1,1]$ using *mapminmax* function in MATLAB, as shown below:

$$x^{i,N}_{j,y,t} = \frac{2(x^i_{j,y,t} - \underline{x^i_{j,y,t}})}{\overline{x^i_{j,y,t}} - \underline{x^i_{j,y,t}}} + \underline{x^{i,N}_{j,y,t}}, \tag{18}$$

  The underline and overline notations denote the respective minimum and maximum values of the inputs.
- Hidden layer activation function: The pre-processed inputs with appropriate weights, $w_{i,o}$ [$\forall i \in 1,...,H$, $o \in 1,...,O$], are summed up at every hidden layer neuron. In addition, each hidden layer neuron has its own bias (β_o). The summed signals present the input to a hidden layer neuron (n^{in}_o), as given below:

$$n^{in}_{o,j,y,t} = \sum_{i=1}^{I} w_{i,o}\, x^{i,N}_{j,y,t} + \beta_o \tag{19}$$

  This input value is passed through an activation function (i.e. $tansig$), which transforms $n^{in}_{o,j,y,t}$ into an output signal ($n^{out}_{o,j,y,t}$), as follows:

$$n^{out}_{o,j,y,t} = \frac{2}{1+\exp\left(-2\, n^{in}_{o,j,y,t}\right)} - 1 \tag{20}$$

- Output layer function: The calculated $n^{out}_{o,j,y,t}$ represents the input of the output layer, which is also multiplied by a layer weight (W_o). Ultimately, a linear function is applied in the output layer, which results in the output of the NN, $X^N_{j,y,t}$, as shown below:

$$X^N_{j,y,t} = \sum_{o}^{O} n^{out}_{o,j,y,t}\, W_o + \Gamma \tag{21}$$

  The obtained output from the NN ($X^N_{j,y,t}$) represents the normalized SoH of the ESS ($SoH^N_{j,y,t}$).
- Post-process output: The obtained output (21) is post-processed to obtain the actual output (i.e. SoH), as follows (refer Fig. 2):

$$X_{j,y,t} = \frac{(X^N_{j,y,t} - \underline{X^N_{j,y,t}})(\overline{X_{j,y,t}} - \underline{X_{j,y,t}})}{2} + \underline{X_{j,y,t}} \tag{22}$$

The mathematical model (22) of the SoH of the ESS at bus j at year y and time t is incorporated in distribution planning model, discussed in the following subsection.

F. LDC Planning Model

The LDC planning model seeks to optimally allocate, size, and replace a number of ESS at different buses in the distribution grid, considering the following objective function.

1) Objective Function:

$$J = J_1 + J_2 + J_3 \tag{23}$$

Equation (23) comprises the ESS installation cost (J_1), operation cost (J_2), and ESS replacement cost (J_3), as follows:

ESS Installation Cost: comprises power capacity cost (\$/*kW*), energy capacity cost (\$/*kWh*), and a fixed

0885-8950 (c) 2020 IEEE. Personal use is permitted, but republication/redistribution requires IEEE permission. See http://www.ieee.org/publications_standards/publications/rights/index.html for more information.
Authorized licensed use limited to: University of Waterloo. Downloaded on April 14,2021 at 09:42:43 UTC from IEEE Xplore. Restrictions apply.

This article has been accepted for publication in a future issue of this journal, but has not been fully edited. Content may change prior to final publication. Citation information: DOI 10.1109/TPWRS.2020.3036448, IEEE Transactions on Power Systems

installation cost ($), as given below:

$$J_1 = \sum_{y=1}^{Y}\sum_{j}^{\mathcal{N}} \left[\frac{1}{(1+R)^y}\,(C_P^{\mathrm{V}}P_{j,y}^{INST}+C_E^{\mathrm{V}}E_{j,y}^{INST}+C^{\mathrm{F}}Z_{j,y}^{INST})\right] \tag{24}$$

Operation Cost: comprises fixed and variable operation and maintenance cost (O&M), the cost associated with ESS charging and discharging, and the cost of buying power from the external grid, as given below:

$$J_2 = \sum_{y=1}^{Y}\sum_{j}^{\mathcal{N}} \left[\frac{C^{\mathrm{OM_F}}}{(1+R)^y}\,P_{j,y}^{Rate} + \frac{365}{\mathrm{DY}}\sum_{t}^{T}\frac{1}{(1+R)^y} \left(C^{\mathrm{OM_V}}(P_{j,y,t}^{CH}+P_{j,y,t}^{DCH}) + \Upsilon_{y,t}P_{j=1,y,t}^{SS})\right)\right] \tag{25}$$

Replacement Cost: included when the ESS reaches its end of life and has to be replaced, as given below:

$$J_3 = \sum_{y=1}^{Y}\sum_{j}^{\mathcal{N}}\frac{C^{\mathrm{REP}}}{(1+R)^y}E_{j,y}^{INST}Z_{j,y}^{REP} \tag{26}$$

The objective function is subject to the following constraints:

2) Selection Decisions of ESS: The selection of the ESS size should be based on standard unit of power and energy capacity ratings available in the market, modeled as follows:

$$E_{j,y}^{INST} = NU^E\ E^{\mathrm{STD}} \tag{27}$$

$$P_{j,y}^{INST} = NU^P\ P^{\mathrm{STD}} \tag{28}$$

NU^E and NU^P are integer variables that determine the rated energy and power capacities respectively, based on the available standard sizes in the market, E^{STD} (e.g. 50 kWh) and P^{STD} (e.g. 50 kW). Furthermore, the energy capacity of the ESS for a certain power rating, is determined based on its energy to power ratio, as follows:

$$\underline{EPR}\ P_{j,y}^{INST} \leq E_{j,y}^{INST} \leq P_{j,y}^{INST}\ \overline{EPR} \tag{29}$$

The installation year decision ($Z_{j,n}^{INST}$) is activated only once during the planning horizon, as indicated below:

$$\sum_{n=1}^{y} Z_{j,n}^{INST} \leq 1 \tag{30}$$

The variable $Z_{j,y}^{PI}$ indicates the presence of ESS after an installation decision. The following constraint coordinates the installation year decision ($Z_{j,n}^{INST}$) in the presence of ESS:

$$Z_{j,y}^{PI} = \sum_{n=1}^{y} Z_{j,n}^{INST} \tag{31}$$

The binary decision variable $Z_{j,y}^{PR}$ indicates the presence of ESS after replacement ($Z_{j,y,t}^{REP}$) and is modeled as follows:

$$Z_{j,y}^{PR} = \sum_{n=1}^{y} Z_{j,n}^{REP} \tag{32}$$

The two binary indicators $Z_{j,y}^{PI}$ and $Z_{j,y}^{PR}$ are used in counting the number of operation years after installation of a new ESS.

The installed energy/power capacity determines the rated capacity of ESS after the year of installation, as follows:

$$E_{j,y}^{Rate} = \sum_{n=1}^{y} E_{j,n}^{INST}\ ;\ P_{j,y}^{Rate} = \sum_{n=1}^{y} P_{j,n}^{INST} \tag{33}$$

It is important to account for ESS energy capacity degradation in order to achieve an optimal plan involving sizing, year, and location of the ESS. Therefore, the de-rated ESS energy capacity can be modeled considering its estimated SoH and rated capacity, as follows:

$$E_{j,y,t} = \widehat{SoH}_{j,y,t}E_{j,y}^{Rate} \tag{34}$$

The following constraint models the estimated SoH of the ESS at installation or replacement, as follows:

$$\widehat{SoH}_{j,y,t=1} \geq Z_{j,y}^{INST} + Z_{j,y}^{REP} \tag{35}$$

It is assumed that ESS installation or replacement is done at the beginning of the year, at which time the battery SoH is 100%; else, $\widehat{SoH}$ is calculated as per Section II-E.

3) Inclusion of SoH Estimator: The first step to estimate the SoH of the ESS is the pre-processing of the required inputs (i.e. $SoC_{j,y,t}$ and $OT_{j,y,t}$). The inputs to the extracted NN mathematical model are normalized and scaled to the range of $[-1, 1]$, as below:

$$SoC_{j,y,t}^{N} = \frac{2(SoC_{j,y,t} - \underline{SoC_j}Z_{j,y}^{PI})}{\overline{SoC} - \underline{SoC_j}} - 1 \tag{36}$$

In (36), $\underline{SoC_j}$ is assumed to be 20% of the ESS installed capacity. $SoC_{j,y,t}^{N} = 1$ when $SoC_{j,y,t} = \overline{SoC}$, and $SoC_{j,y,t}^{N} = -1$ when $Z_{j,y}^{PI} = 0$. Similarly, the following equation normalizes the operation time of the ESS.

$$OT_{j,y,t}^{N} = \frac{2\ OT_{j,y,t}}{T} - 1 \tag{37}$$

where,

$$OT_{j,y,t} = HY(OY_{j,y} - Z_{j,y}^{PI}) + (t-1)Z_{j,y}^{PI} \tag{38}$$

In (38), the first term on the RHS denotes the total number of ESS operational hours from installation/replacement until the previous year, while the second term denotes the number of hours of operation in the current year. Furthermore, note that $OY_{j,y}$ is a function of installation and replacement decisions, which represents the total number of years of operation after ESS is installed/replaced, as follows:

$$OY_{j,y} \leq \sum_{n=1}^{y} Z_{j,n}^{PI} + M\sum_{n=1}^{y} Z_{j,n}^{REP} \tag{39}$$

$$OY_{j,y} \geq \sum_{n=1}^{y} Z_{j,n}^{PI} - M\sum_{n=1}^{y} Z_{j,n}^{REP} \tag{40}$$

$$OY_{j,y} \leq \sum_{n=1}^{y} Z_{j,n}^{PR} + M(1 - \sum_{n=1}^{y} Z_{j,n}^{REP}) \tag{41}$$

$$OY_{j,y} \geq \sum_{n=1}^{y} Z_{j,n}^{PR} - M(1 - \sum_{n=1}^{y} Z_{j,n}^{REP}) \tag{42}$$

0885-8950 (c) 2020 IEEE. Personal use is permitted, but republication/redistribution requires IEEE permission. See http://www.ieee.org/publications_standards/publications/rights/index.html for more information.
Authorized licensed use limited to: University of Waterloo. Downloaded on April 14,2021 at 09:42:43 UTC from IEEE Xplore. Restrictions apply.

This article has been accepted for publication in a future issue of this journal, but has not been fully edited. Content may change prior to final publication. Citation information: DOI 10.1109/TPWRS.2020.3036448, IEEE Transactions on Power Systems

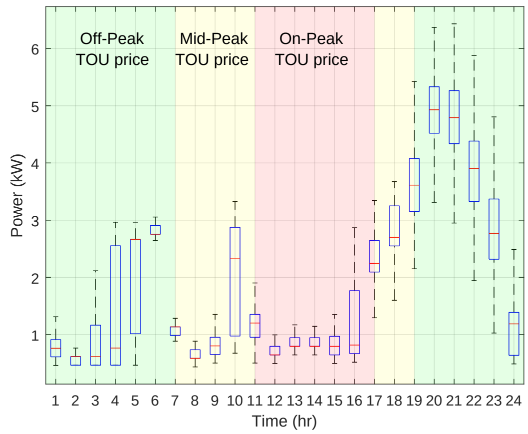

Fig. 3. Residential load profile.

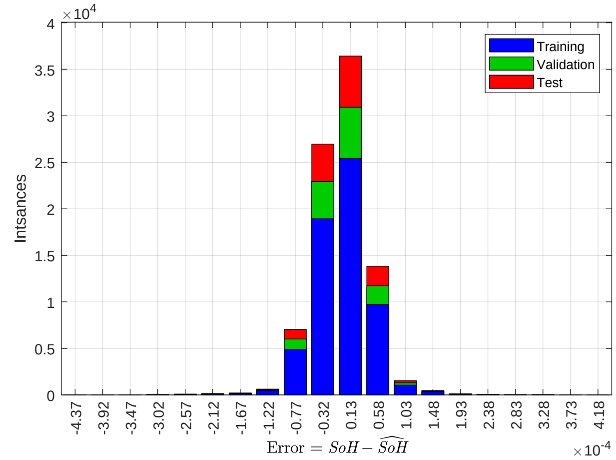

Fig. 4. Training, validation, testing histogram of NN-based SoH estimator.

TABLE I
TUNED WEIGHTS AND BIASES OF THE NN

Parameter	Hidden Layer				Output Layer	
Weight	w_{11}	$-0.164E-4$	w_{12}	0.2218	W_1	-0.4328
	w_{21}	$0.447E-6$	w_{22}	-0.0661	W_2	-16.5719
Bias	β_1	$-0.5117E-2$	β_1	$0.3317E-3$	Γ	$0.3260E-2$

Equations (39) and (40) coordinate the counting of $OY_{j,y,t}$ for an ESS in service after installation, while (41) and (42) counts the number of years an ESS is in service after a replacement.

The normalized inputs (i.e. $SoC^N_{j,y,t}$ and $OT^N_{j,y,t}$) are passed to the hidden layer of the NN, as follows:

$$n^{out}_{o,j,y,t} = \frac{2}{1+e^{-2\,(w_{1,o}\ SoC^N_{j,y,t}+w_{2,o}\ OT^N_{j,y,t}+\beta_o)}} - 1 \tag{43}$$

Finally, $\widehat{SoH}^N_{j,y,t}$, which is the normalized output of the NN, can be expressed as follows:

$$\widehat{SoH}^N_{j,y,t} = \sum_{o\in O} n^{out}_{o,j,y,t}\ W_o + \Gamma \tag{44}$$

4) Budget Constraint: The net present value (NPV) of the installation cost should not exceed the NPV of the allocated budget:

$$J_1 \leq Budget \tag{45}$$

The constraints of the LDC operations model, discussed in Section II-B (i.e. (2) to (13)), are further included in the planning model in addition to the above constraints.

III. RESULTS AND DISCUSSIONS

In this work, a 33-bus test system is used to determine the optimal ESS size, location, and year of installation / replacement considering the impact of its calendar and cycle aging on its SoH. The residential load demand is assumed to increase 3% annually. The planning period is 10 years; each year is represented by one day, and each day's operational aspects, such as load and generation profiles and charge / discharge decisions, are modeled hourly. The representative day is the one which has the highest peak demand of that year. This is a conservative approach, using the worst-case scenario and planning accordingly, so that the system has sufficient redundancy and margin. The choice of one representative day per year reduces the computational burden of the planning model.

To implement the planning framework proposed in Fig. 1, 2,600 individual REH operations models [1] are executed to obtain their daily optimal load profiles, and hence the LDC's load profiles at each bus are created. Fig. 3 shows the distribution of the REH loads at each hour, indicating the minimum and maximum, 25$^{\text{th}}$ and 75$^{\text{th}}$ percentiles, and the median consumption of the customers. Note that during the on-peak TOU prices, the variation in customer load is small, which depicts harmonized operation of REHs. The HEMS helps the household in shifting its demand from on-peak TOU price to off-peak price hours.

The LDC operations model is executed for (365 x 10 days) considering the respective REH load profiles to obtain the corresponding optimal SoC profiles of the ESS. This data set is divided into a training set (60%), validation set (20%), and testing set (20%). The *Dividerand* function of the MATLAB NN-Toolbox [24] is applied to divide the data set using random indices. The training stage takes place to build the NN-based SoH estimator. Fig. 4 presents the error distribution between $SoH_{j,y,t}$ and $\widehat{SoH}$ with the number of incidences. The main outcomes of the NN, as stated in Fig. 1, are the input weights, layer weights, and biases at hidden and output layer neurons. Table I shows the resulting parameters of the NN, which are used to construct the SoH functional relation given in (44).

Next, the proposed LDC planning model is executed to obtain the optimal ESS plan decisions over the 10 year horizon including ESS energy and power capacity, location, and installation years, considering the following case studies:

- Case-1: Proposed SoH-integrated LDC planning model.
- Case-2: Without degradation of ESS.
- Case-3: Fixed annual degradation rate of 5%.

Furthermore, each case has been studied considering four load profile scenarios:

0885-8950 (c) 2020 IEEE. Personal use is permitted, but republication/redistribution requires IEEE permission. See http://www.ieee.org/publications_standards/publications/rights/index.html for more information.
Authorized licensed use limited to: University of Waterloo. Downloaded on April 14,2021 at 09:42:43 UTC from IEEE Xplore. Restrictions apply.

This article has been accepted for publication in a future issue of this journal, but has not been fully edited. Content may change prior to final publication. Citation information: DOI 10.1109/TPWRS.2020.3036448, IEEE Transactions on Power Systems

TABLE II
ESS OPTIMAL PLAN (CONSIDERING SCENARIO-1 LOAD PROFILE).

Case Study	Optimal Plan Decisions*		Operation Cost (NPV-OC)	Installation Cost (NPV-OC)
Case-1 (Proposed Approach)	(2, 9, 400, 1500) (8, 4, 150, 600) (19, 5, 500, 2000) (30, 6, 250, 1000)	(4, 5, 450, 1800) (17, 7, 400, 1600) (23, 10, 500, 2000)	$64,000	$5,988,000
	Total Rated Power/Energy: 2.65 MW/10.5 MWh		Total: $6,052,000	
Case-2 (Without Degradation)	(2, 7, 300, 1200) (8, 5, 500, 2000) (17, 4, 200, 800) (23, 5, 150, 600)	(4, 5, 500, 2000) (15, 9, 250, 1000) (19, 10, 300, 1150) (30, 6, 250, 1000)	$68,000	$5,815,000
	Total Rated Power/Energy: 2.5 MW/9.75 MWh		Total: $5,881,000	
Case-3 (Fixed Degradation Rate)	(2, 5, 500, 2000) (8, 7, 250, 1000) (17, 6, 250, 1000) (23, 4, 400, 1600)	(4, 10, 400, 1600) (15, 9, 400, 1600) (19, 8, 250, 1000) (30, 5, 500, 2000)	$77,000	$6,844,000
	Total Rated Power/Energy: 2.95 MW/11.8 MWh		Total: $6,921,000	

*(Bus number, Year of Installation, Rated Power (kW), Rated Energy (kWh))

TABLE III
ESS OPTIMAL PLAN USING THE PROPOSED APPROACH (CASE-1) FOR DIFFERENT LOAD PROFILE SCENARIOS

	Optimal Plan Decisions*	
Scenario-1 IEEE RTS Load	(2, 9, 400, 1500) (8, 4, 150, 600) (19, 5, 500, 2000) (30, 6, 250, 1000)	(4, 5, 450, 1800) (17, 7, 400, 1600) (23, 10, 500, 2000)
	Total: 2.65 MW/10.5 MWh	
Scenario-2 50% IEEE RTS load 50% REH penetration	(2, 5, 600, 2000) (8, 10, 350, 1400) (23, 9, 250, 1000)	(4, 3, 950, 1550) (19, 7, 150, 600)
	Total: 2.3 MW/6.55 MWh	
Scenario-3 IEEE RTS Load 20% PV penetration (-ve load)	(4, 5, 500, 2000) (15, 5, 450, 1800) (19, 10, 350, 1400)	(8, 4, 150, 600) (17, 8, 500, 2000) (23, 6, 350, 1400)
	Total: 2.3 MW/9.2 MWh	
Scenario-4 50% IEEE RTS load 50% REH penetration 20% PV penetration (-ve load)	(2, 4, 550, 1900) (19, 5, 700, 2000) (30, 7, 300, 1200)	(17, 10, 350, 1400) (23, 3, 250, 300)
	Total: 2.15 MW/6.8 MWh	

*(Bus number, Year of Installation, Rated Power (kW), Rated Energy (kWh))

TABLE IV
NPV OF OPERATION AND INSTALLATION COSTS FOR VARIOUS CASES AND SCENARIOS ($1000)

Case	Scenario-1		Scenario-2		Scenario-3		Scenario-4	
	NPV-OC	NPV-IC	NPV-OC	NPV-IC	NPV-OC	NPV-IC	NPV-OC	NPV-IC
1	64	5,988	65	4,800	62	5,364	69	4,630
2	68	5,815	66	4,106	53	5,264	68	4,038
3	77	6,844	76	4,980	68	6,142	69	4,772

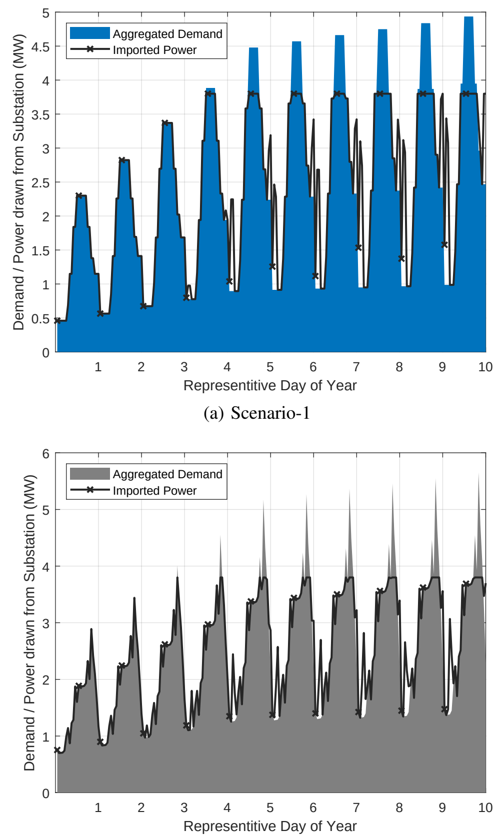

(a) Scenario-1

(b) Scenario-2

Fig. 5. Total distribution system demand and power drawn from substation for Case-1 (Proposed Approach) over the planning period.

- Scenario-1: System demand profile is modeled using the IEEE RTS load.
- Scenario-2: System demand profile is a mix of 50% penetration of REHs and rest modeled using the IEEE RTS load.
- Scenario-3: System demand profile is a mix of 20% penetration of PVs and rest modeled using the IEEE RTS load.
- Scenario-4: System demand profile is a mix of 50% penetration of REHs, 20% penetration of PVs, and rest modeled using the IEEE RTS load.

Two load profiles are used: IEEE RTS load and REHs. Assuming that the connected load of an REH is 3 kW, the number of REHs connected at a bus is determined by dividing the IEEE RTS peak load at a bus by 3 kW. Each REH model is then executed to build a bus-wise load profile [1]. The total demands of Scenario-1 and Scenario-2 are shown in Fig. 5. In Scenario-3 and Scenario-4, it is assumed that PV facilities are commissioned at buses 3, 17, and 30 in

0885-8950 (c) 2020 IEEE. Personal use is permitted, but republication/redistribution requires IEEE permission. See http://www.ieee.org/publications_standards/publications/rights/index.html for more information.
Authorized licensed use limited to: University of Waterloo. Downloaded on April 14,2021 at 09:42:43 UTC from IEEE Xplore. Restrictions apply.

This article has been accepted for publication in a future issue of this journal, but has not been fully edited. Content may change prior to final publication. Citation information: DOI 10.1109/TPWRS.2020.3036448, IEEE Transactions on Power Systems

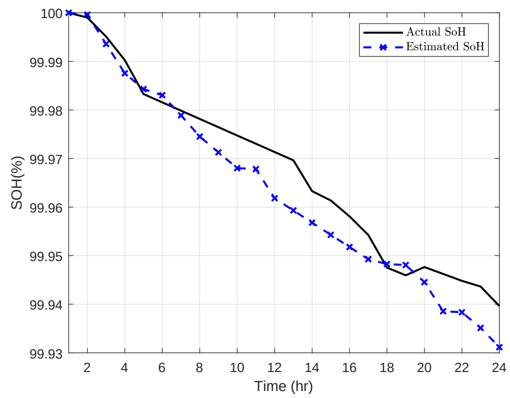

Fig. 6. SoH profile of ESS located at Bus-8 over a day.

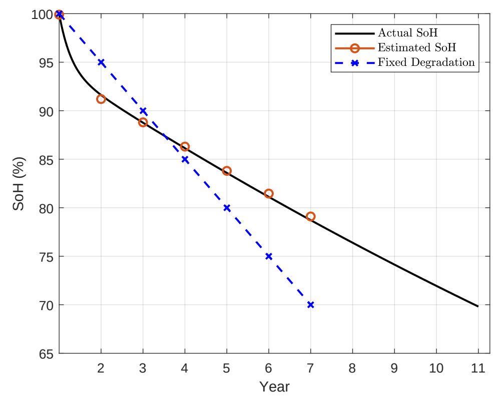

Fig. 7. SoH profile of ESS located at Bus-8 over the operation period.

years 3, 6, and 8, respectively, with their power capacity being 20% of the load at that bus. Note that, in the system load profile, the PVs appear as a negative load.

The case studies, Table II, examine the impact the proposed approach vs less accurate SoH models in LDC planning framework while the (load profile) scenarios, Table III, examine the impact of load mix and PV penetration on ESS sizing, siting, and year of installation / replacement. These tables also show the optimal ESS planning combinations for each scenario and case; and Table IV shows the associated operation and installation cost NPVs.

It is seen from Table II that in Case-1, the LDC needs to invest in a total ESS capacity of 2.65 MW/10.5 MWh across seven ESS units. The NPV of the ESS installation cost is M$5.99. In Case-2, eight ESS units are invested in by the LDC although the total ESS capacity is 2.5 MW, 9.75 MWh for a total cost that is 2.8% lower than Case-1. This is because the SoH of the ESS units are considered to remain unchanged in Case-2. On the other hand, Case-3 requires 2.95 MW, 11.8 MWh of ESS capacity when using a fixed-rate degradation.

Table III shows the LDC optimal plan for the four scenarios. In the first scenario, the total capacity of ESS units is higher than Scenario-2 as a consequence of the former's longer duration of peak demand (Fig. 5). In Scenario-3, the integration of PV results in an approx. 10% reduction in installed ESS capacity compared to Scenario-1.

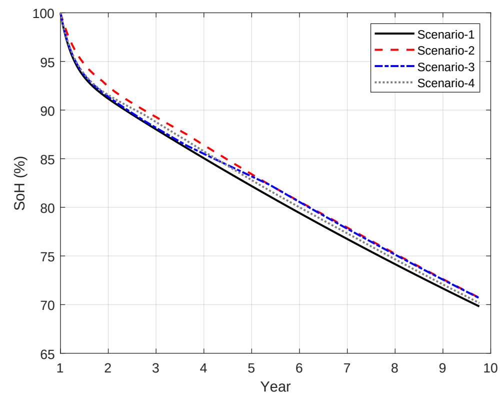

Fig. 8. SoH profiles of optimal ESS at Bus-23 in Case-1 for various scenarios.

However, the integration of PV units does not significantly influence the decisions of ESS in the presence of REHs, as seen comparing Scenario-2 with Scenario-4, because the maximum PV power output occurs during the mid-day and does not coincide with the peak demand of the uncoordinated REHs which appear at the onset of off-peak TOU prices.

Scenario-1 has total LDC NPV costs around M$6.05, M$5.88, and M$6.92 for Case-1, Case-2, and Case-3, respectively (Table IV). On average, LDC cost in Case-2 is around 8% lower than in Case-1 since, for the former, ESS SoH is fixed at 100%, which results in over-estimation of the available energy capacity of the Li-ion batteries. On the other hand, in Case-3, the average LDC cost is around 10% higher than Case-1 because of the under-estimation of ESS SoH when using the fixed-rate degradation, leading to higher operation and installation costs.

Fig. 6 shows the SoH and $\widehat{SoH}$ profiles of the ESS located at bus-8 over a 24-hour operation considering the proposed degradation model of Case-1. It is noted that the proposed NN-based mathematical model captures the hourly SoH profile ($\widehat{SoH}$) due to calendar and cycle aging with a relatively small error, as compared to SoH.

Fig. 7 shows the actual SoH, $SoH_{j,y,t}$, the estimated SoH from Case-1, $\widehat{SoH}$, and the SoH profile considering a fixed deterioration of 5%, as in Case-3, over the plan period. $SoH_{j,y,t}$ is obtained using the off-line degradation model proposed in [19] and discussed in Section II-D. In contrast, the $\widehat{SoH}$ profile is calculated using the proposed NN-based SoH estimator model, which is shown precise compared to $SoH_{j,y,t}$.

$SoH_{j,y,t}$ obtained from the different load mix scenarios are shown in Fig. 8; Scenario-1 has consistently the lowest SoH. It is noted that the load mix has some influence on the battery degradation: the penetration of PV units and the presence of REHs improve the overall SoH of Li-ion batteries by around 1% every year, as a consequence of the adoption of RES or REH, which results in a reduction in the peak duration of the system load and requires steep discharge from ESS.

Fig. 5 shows the LDC's aggregated system demand and the power it imports over the substation in Scenarios-1 and -2 for the representative day in each planning year. The ESS units

0885-8950 (c) 2020 IEEE. Personal use is permitted, but republication/redistribution requires IEEE permission. See http://www.ieee.org/publications_standards/publications/rights/index.html for more information.
Authorized licensed use limited to: University of Waterloo. Downloaded on April 14,2021 at 09:42:43 UTC from IEEE Xplore. Restrictions apply.

This article has been accepted for publication in a future issue of this journal, but has not been fully edited. Content may change prior to final publication. Citation information: DOI 10.1109/TPWRS.2020.3036448, IEEE Transactions on Power Systems

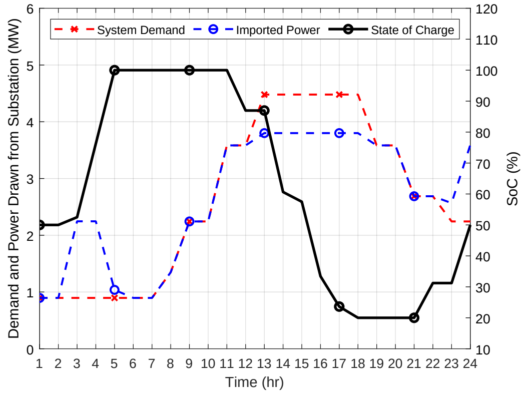

(a) Scenario-1

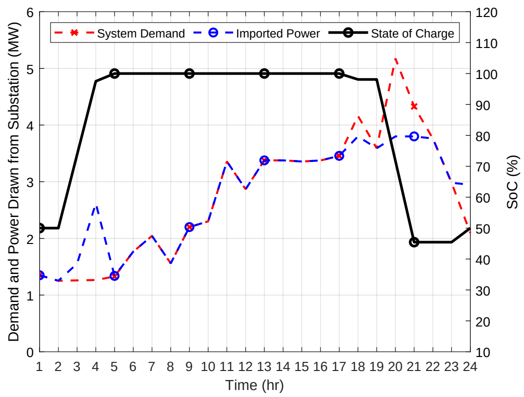

(b) Scenario-2

Fig. 9. Total demand, power imported from external grid, and ESS operation over one-day of year-10.

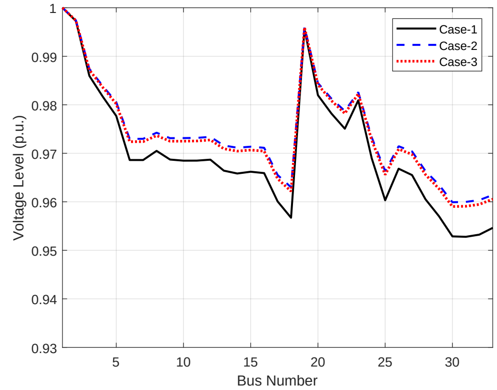

(a) Scenario-1

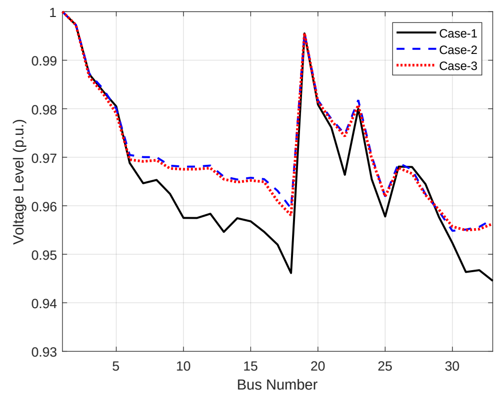

(b) Scenario-2

Fig. 10. System voltage profiles for different case studies, for Scenario-1 and -2, during peak demand in the terminal year.

supply the net difference between demand and imports. Fig. 9 shows the total demand and power imported from external grid over a day in the last year of the planning period for Scenario-1 and -2. The SoC of ESS located at bus 23 is also included, which shows high / low SoC during low / high RTS and REH demand, respectively.

Fig. 10 shows the bus voltage profiles during peak demand hours: hour-18 in Scenario-1 and hour-20 in Scenario-2 of the terminal year. Note that the voltages are always within pre-specified limits (i.e. 0.9 to 1.0 $p.u.$). Scenario-2 shows a higher deviation in voltage from the nominal value of 1.0 $p.u.$ as compared to Scenario-1 as a consequence of the higher demand from mixed loads in the former. The voltage profile in Case-1 is also lower in Scenarios-1 and -2 than the voltage profiles in Case-2 and -3.

IV. Conclusions

A novel NN-based SoH estimator was developed using a large cluster of smart loads, simulated to represent the total load of the distribution grid; and a large data set of ESS operations, simulated to mimic the LDC's behavior in controlling the ESSs. Hence extracted functional relationship of SoH was integrated within a distribution planning model, which included a large penetration of smart REHs. The NN model was re-trained using the updated outcomes of the planning model to improve the plan decisions. The results showed a relatively small error between the estimated and the actual SoH of ESS. The case studies demonstrated the impact of neglecting calendar and cycle aging and under- / over-estimation of the ESS capacity on the plan decisions of the LDC.

References

[1] O. Alrumayh and K. Bhattacharya, "Flexibility of residential loads for demand response provisions in smart grid," *IEEE Trans. Smart Grid*, vol. 10, no. 6, pp. 6284–6297, Nov 2019.

[2] D. J. Olsen, M. R. Sarker, and M. A. Ortega-Vazquez, "Optimal penetration of home energy management systems in distribution networks considering transformer aging," *IEEE Trans. Smart Grid*, vol. 9, no. 4, pp. 3330–3340, July 2018.

[3] A. Taşcıkaraoğlu, N. G. Paterakis, O. Erdinç, and J. P. S. Catalão, "Combining the flexibility from shared energy storage systems and dlc-based demand response of hvac units for distribution system operation enhancement," *IEEE Trans. Sustainable Energy*, vol. 10, no. 1, pp. 137–148, 2019.

[4] P. Ju, T. Jiang, H. Li, C. Wang, and J. Liu, "Hierarchical control of air-conditioning loads for flexible demand response in the short term," *IEEE Access*, vol. 7, pp. 184 611–184 621, 2019.

[5] H. Kikusato, K. Mori, S. Yoshizawa, Y. Fujimoto, H. Asano, Y. Hayashi, A. Kawashima, S. Inagaki, and T. Suzuki, "Electric vehicle charge–discharge management for utilization of photovoltaic by coordination between home and grid energy management systems," *IEEE Trans. Smart Grid*, vol. 10, no. 3, pp. 3186–3197, 2019.

[6] B. Celik, R. Roche, D. Bouquain, and A. Miraoui, "Decentralized neighborhood energy management with coordinated smart home energy sharing," *IEEE Trans. Smart Grid*, vol. 9, no. 6, pp. 6387–6397, 2018.

0885-8950 (c) 2020 IEEE. Personal use is permitted, but republication/redistribution requires IEEE permission. See http://www.ieee.org/publications_standards/publications/rights/index.html for more information.
Authorized licensed use limited to: University of Waterloo. Downloaded on April 14,2021 at 09:42:43 UTC from IEEE Xplore. Restrictions apply.

This article has been accepted for publication in a future issue of this journal, but has not been fully edited. Content may change prior to final publication. Citation information: DOI 10.1109/TPWRS.2020.3036448, IEEE Transactions on Power Systems

[7] V. C. Cunha, R. Torquato, T. R. Ricciardi, W. Freitas, and B. Venkatesh, "Assessing energy storage potential to facilitate the increased penetration of photovoltaic generators and electric vehicles in distribution networks," in *2017 IEEE Power Energy Society General Meeting*, July 2017, pp. 1–5.

[8] R. Li, W. Wang, and M. Xia, "Cooperative planning of active distribution system with renewable energy sources and energy storage systems," *IEEE Access*, vol. 6, pp. 5916–5926, 2018.

[9] S. Wen, H. Lan, Q. Fu, D. C. Yu, and L. Zhang, "Economic allocation for energy storage system considering wind power distribution," *IEEE Trans. Power Syst.*, vol. 30, no. 2, pp. 644–652, 2015.

[10] M. Sedghi, A. Ahmadian, and M. Aliakbar-Golkar, "Optimal storage planning in active distribution network considering uncertainty of wind power distributed generation," *IEEE Trans. Power Syst.*, vol. 31, no. 1, pp. 304–316, 2016.

[11] A. S. A. Awad, T. H. M. EL-Fouly, and M. M. A. Salama, "Optimal ess allocation for load management application," *IEEE Trans. Power Syst.*, vol. 30, no. 1, pp. 327–336, 2015.

[12] H. Hamidpour, J. Aghaei, S. Pirouzi, S. Dehghan, and T. Niknam, "Flexible, reliable, and renewable power system resource expansion planning considering energy storage systems and demand response programs," *IET Renewable Power Generation*, vol. 13, no. 11, pp. 1862–1872, 2019.

[13] H. Akhavan-Hejazi and H. Mohsenian-Rad, "Energy storage planning in active distribution grids: A chance-constrained optimization with non-parametric probability functions," *IEEE Trans. Smart Grid*, vol. 9, no. 3, pp. 1972–1985, May 2018.

[14] F. Luo, K. Meng, Z. Y. Dong, Y. Zheng, Y. Chen, and K. P. Wong, "Coordinated operational planning for wind farm with battery energy storage system," *IEEE Trans. Sustainable Energy*, vol. 6, no. 1, pp. 253–262, 2015.

[15] T. Qiu, B. Xu, Y. Wang, Y. Dvorkin, and D. S. Kirschen, "Stochastic multistage coplanning of transmission expansion and energy storage," *IEEE Trans. Power Syst.*, vol. 32, no. 1, pp. 643–651, Jan 2017.

[16] H. Alharbi and K. Bhattacharya, "Stochastic optimal planning of battery energy storage systems for isolated microgrids," *IEEE Trans. Sustain. Energy*, vol. 9, no. 1, pp. 211–227, Jan 2018.

[17] I. Alsaidan, A. Khodaei, and W. Gao, "A comprehensive battery energy storage optimal sizing model for microgrid applications," *IEEE Trans. Power Syst.*, vol. 33, no. 4, pp. 3968–3980, 2018.

[18] T. Alharbi, K. Bhattacharya, and M. Kazerani, "Planning and operation of isolated microgrids based on repurposed electric vehicle batteries," *IEEE Trans. Ind. Informat.*, vol. 15, no. 7, pp. 4319–4331, July 2019.

[19] B. Xu, A. Oudalov, A. Ulbig, G. Andersson, and D. S. Kirschen, "Modeling of lithium-ion battery degradation for cell life assessment," *IEEE Trans. Smart Grid*, vol. 9, no. 2, pp. 1131–1140, March 2018.

[20] H. Yuan, F. Li, Y. Wei, and J. Zhu, "Novel linearized power flow and linearized opf models for active distribution networks with application in distribution lmp," *IEEE Trans. Smart Grid*, vol. 9, no. 1, pp. 438–448, Jan 2018.

[21] C. Amzallag, J. Gerey, J. Robert, and J. Bahuaud, "Standardization of the rainflow counting method for fatigue analysis," *International journal of fatigue*, vol. 16, no. 4, pp. 287–293, 1994.

[22] Y. Niu and S. Santoso, "Sizing and coordinating fast- and slow-response energy storage systems to mitigate hourly wind power variations," *IEEE Trans. Smart Grid*, vol. 9, no. 2, pp. 1107–1117, 2018.

[23] B. Vatandoust, A. Ahmadian, M. A. Golkar, A. Elkamel, A. Almansoori, and M. Ghaljehei, "Risk-averse optimal bidding of electric vehicles and energy storage aggregator in day-ahead frequency regulation market," *IEEE Trans. Power Syst.*, vol. 34, no. 3, pp. 2036–2047, 2019.

[24] M. H. Beale, M. T. Hagan, and H. B. Demuth, "Neural network toolbox™ user's guide," *The MathWorks*, 2010.

Omar Alrumayh (S'15) received the B.Sc. degree in electrical engineering from Qassim University, Saudi Arabia, in 2011, and M.A.Sc degree in electrical and computer engineering (ECE) from University of Waterloo, ON, Canada, in 2016, where he is currently pursuing the Ph.D. degree. He is also a Lecturer with the Department of Electrical Engineering, Qassim University. His research interests include power system operations, energy management, energy storage systems, and smart grids.

Steven Wong (S'05–M'12) was born in Canada. He received the B.A.Sc. degree in electrical engineering, the M.A.Sc. degree in management sciences, and the Ph.D. in electrical engineering, all from the University of Waterloo, Waterloo, ON, Canada, in 2003, 2005, and 2009, respectively.

He joined CanmetENERGY, Natural Resources Canada, Varennes, QC, Canada, in 2010. He is also an adjunct associate professor at the University of Waterloo, Waterloo, ON, Canada. He advises and conducts research into the integration of renewable and distributed energy resources, smart grid, and electrification.

Kankar Bhattacharya (M'95–SM'01–F'17) received the Ph.D. degree in electrical engineering from Indian Institute of Technology, New Delhi, India, in 1993. He was with the Faculty of Indira Gandhi Institute of Development Research, Mumbai, India, from 1993 to 1998, and with the Department of Electric Power Engineering, Chalmers University of Technology, Gothenburg, Sweden, from 1998 to 2002. In 2003, he joined the Electrical and Computer Engineering Department, University of Waterloo, Waterloo, ON, Canada, where he is currently a Full Professor. His research interests include power system economics and operational aspects. He is a Registered Professional Engineer in the province of Ontario.

0885-8950 (c) 2020 IEEE. Personal use is permitted, but republication/redistribution requires IEEE permission. See http://www.ieee.org/publications_standards/publications/rights/index.html for more information.
Authorized licensed use limited to: University of Waterloo. Downloaded on April 14,2021 at 09:42:43 UTC from IEEE Xplore. Restrictions apply.